SIMULATING THE LIAISON NAVIGATION CONCEPT IN A GEO + EARTH-MOON HALO CONSTELLATION

K. Fujimoto[(1)], J. M. Leonard[(2)], R. M. McGranaghan[(3)], J. S. Parker[(4)], R. L. Anderson[(5)], and G. H. Born[(6)]

[(1)(2)(3)(4)(6)]*Department of Aerospace Engineering Sciences, The University of Colorado-Boulder, ECEE 166, 431 UCB, Boulder, CO 80309-0431 USA, +1-(303)-492-7826, kohei.fujimoto@colorado.edu*

[(5)]*Member of Technical Staff, Jet Propulsion Laboratory, California Institute of Technology, 4800 Oak Grove Drive, M/S 301-121, Pasadena, CA 91109 USA, +1-(818)-393-6675, Rodney.L.Anderson@jpl.nasa.gov*

Abstract: *Linked Autonomous Interplanetary Satellite Orbit Navigation, or LiAISON, is a novel satellite navigation technique where relative radiometric measurements between two or more spacecraft in a constellation are processed to obtain the absolute state of all spacecraft. The method leverages the asymmetry of the gravity field that the constellation exists in. This paper takes a step forward in developing a high fidelity navigation simulation for the LiAISON concept in an Earth-Moon constellation. In particular, we aim to process two-way Doppler measurements between a satellite in GEO orbit and another in a halo orbit about the Earth-Moon L_1 point.*

Keywords: *Autonomous Navigation, Satellite-to-Satellite Tracking, Orbit Determination, LiAISON.*

1. Introduction

Linked Autonomous Interplanetary Satellite Orbit Navigation, or LiAISON, is a novel satellite navigation technique where relative radiometric measurements between two or more spacecraft in a constellation are processed to obtain the absolute state of all spacecraft [1–5]. No ground-based measurements are required. The method leverages the asymmetry of the gravity field that the constellation exists in, allowing a unique configuration to exist. Previous research has focused on lunar constellations with at least one satellite in an Earth-Moon libration point orbit; LiAISON, however, is not confined to this particular set up, and could be of use in other navigation scenarios, as suggested by Hill [1]. One scenario of interest is to apply LiAISON to GEO satellites as traditional ground-based orbit determination in this orbit regime is often difficult due to a lack of relative motion and conventional GPS receivers are ineffective at such high altitudes. This configuration would extend a GPS-like navigation capability to any Earth orbiting satellite as well as those at the Moon. Although the current work focuses on the tracking of a GEO satellite, it has implications for other Earth or Moon orbits.

This paper takes a step forward in developing a high fidelity navigation simulation for the LiAISON concept in an Earth-Moon constellation, with one satellite in GEO orbit and another in a halo orbit about the Earth-Moon L_1 point. In particular, we aim to process two-way Doppler measurements modeled as a discrete change in the roundtrip light path length. Again, only relative measurements between the two satellites are processed as observations. The overall structure of the paper is as follows. First, the LiAISON concept and the observation / dynamical model employed in this paper are introduced (Section 2.). As a baseline scenario, navigation results in the circular restricted

three-body problem are discussed. Then, the details of the simulations run for this paper are presented (Section 3.). An extended Kalman filter processes observations corrupted by noise and a constant bias consistent with S- and X-band measurements. An initial state deviation and dynamical modeling errors are also added to the problem. Finally, the navigation results are shown (Section 4.). LiAISON navigation succeeds in extracting absolute state information based on simulated Doppler measurements, although including range-type measurements would further improve filter convergence.

2. Background

In this section, we qualitatively introduce the LiAISON navigation concept through a baseline simulation utilizing idealized dynamics. We then explain the measurement and dynamical models implemented in the current paper. Refer to Parker, et al. and Leonard, et al. for a more detailed treatment [4, 5].

2.1. LiAISON in the Earth-Moon System

Autonomous satellite-to-satellite tracking relies on an ability to estimate the absolute positions of a spacecraft without the use of groundstation observations. To do so, the size, shape, and orientation of the satellites orbit must be observable from the measurements available between the linked spacecraft. The observability of the system depends on one of these satellites occupying a unique trajectory. The determining factor in whether a unique trajectory can exist, and thus whether LiAISON is possible, is the acceleration function acting on the orbiter. No unique orbits exist in a symmetric acceleration field, one in which the function and its time derivative are symmetric. Even in regions with desired asymmetric perturbations, uncertainties in the force model and observation noise can counteract these effects in the accelerations and prevent satellite-to-satellite tracking (SST) orbit determination. As a result, the asymmetric acceleration effects must be great enough to outweigh the uncertainties and force model issues that arise.

Acceleration functions with sufficient asymmetry for LiAISON are provided by three-body systems that give rise to libration point orbits (LPOs). Third-body perturbation of the Moon are sufficient to provide the asymmetry necessary for locally unique trajectories to exist. Due to the effects of the gravitational forces of the Moon and Earth, lunar LPOs can only have one orientation with respect to this system. L_1 LPOs are specifically well suited for LiAISON because they are locally unique and reside in regions where the asymmetry of the accelerations is strong. Under these conditions a spacecraft at L_1 can uniquely and absolutely determine the state of a second satellite using crosslink measurements without ground-based observations.

The scenario examined in this paper extends the concepts of LiAISON navigation beyond constellations fixed at the Moon [1, 2, 6, 7]. This study considers placing one satellite in a GEO orbit, since there is significant interest in improving the navigation of GEO satellites; future studies will examine other orbits, including low Earth orbits, lunar transfers, and interplanetary trajectories. It may be the case that NASA's lunar development warrants a dedicated navigation satellite; this study demonstrates that such a satellite may be able to offer substantial benefits to Earth-orbiting satellites as well.

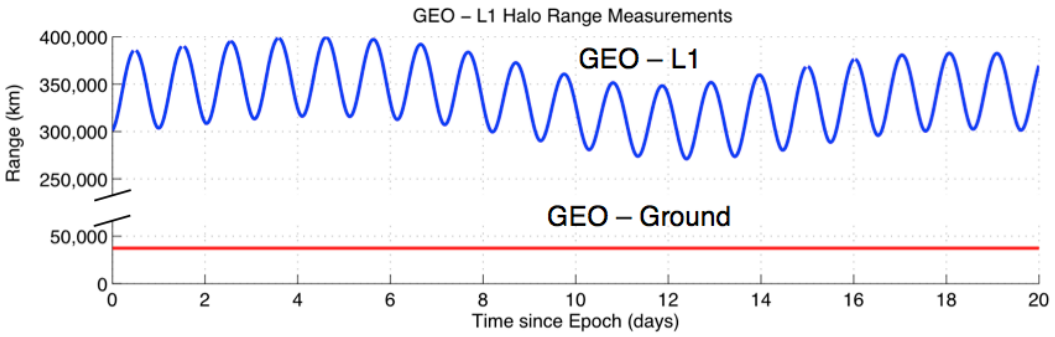

Figure 1. Satellite constellation geometry for truth model simulations for LiAISON and ground-tracking [5].

The effectiveness of the autonomous satellite tracking system is evaluated using orbit determination solely composed of relative measurements between two participating spacecraft. A dedicated navigation satellite anywhere near the Moon has an advantage over groundstations for tracking GEO satellites using radiometric data. Figure 1 demonstrates the dynamic range measurements between an example GEO satellite and a satellite traversing an LPO about the Earth-Moon L_1 point versus the range of a GEO orbit tracked by a groundstation. One can see clear signals in the data that may be used to lock onto the position and velocity of both satellites.

As a baseline case, we present here LiAISON navigation results between one satellite in a lunar L_1 LPO and another at GEO simulated in the circular restricted three-body problem (CRTBP). The CRTBP models the motion of a massless particle, e.g., a spacecraft, in the presence of two massive bodies, e.g., the Earth and the Moon, where the two massive bodies are in circular orbits about their barycenter. The analysis presented here uses values for the gravitational parameters of the Earth and Moon of 398,600.4415 km^3/s^2 and 4902.80 km^3/s^2, respectively. The initial state deviation is 100 meters in position and 1 cm/s in velocity for both satellites. The a priori covariance is set to correspond with the initial state deviation: it has been set to a diagonal matrix with values of 10^4 m^2 in position and 10^{-2} $(\text{m/s})^2$ in velocity for both satellites. State noise compensation has been implemented with a 1-σ value of 1×10^{-13} m/s^2 for the halo orbiter and 1×10^{-14} m/s^2 for the GEO satellite on the diagonal of the a priori process noise covariance matrix. Simulated instantaneous relative range and range-rate measurements with 1 meter and 1 cm/s 1-σ noise, respectively, were processed every 100 seconds with an extended Kalman filter (EKF).

Figure 2 illustrates the time evolution of the position and velocity accuracy of the simulation as the EKF processes the observations, namely, the difference between the truth trajectory and the estimated trajectory over time. Figure 3 presents the components of the covariance matrix over time on a logarithmic axis for clarity. One can see that the uncertainty of the position of either satellite converges to about one meter within about eight days. The coordinates are represented in the Earth-Moon rotating coordinate frame. The largest off-diagonal element in the variance-covariance matrix after 9 days of processing has a value of approximately 1.1×10^{-17}, illustrating that there is no correlation in the state variables. The post-fit range residuals have an RMS of approximately 0.99519 meters.

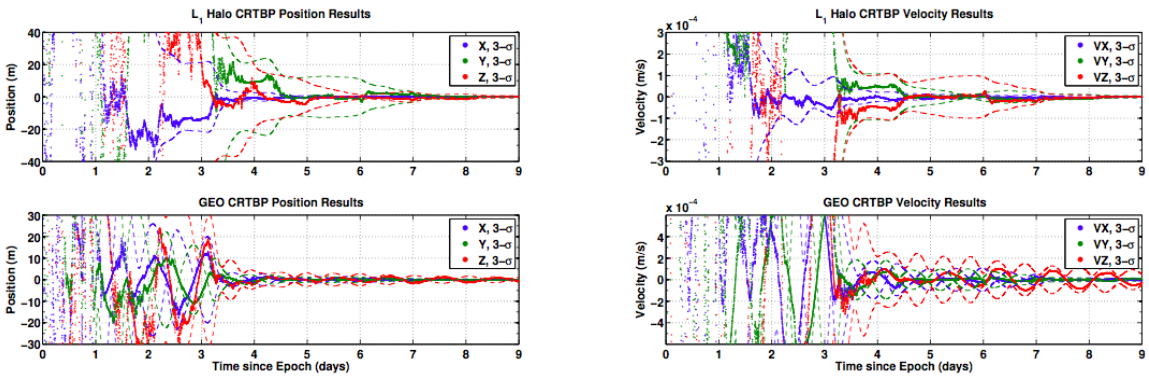

Figure 2. Time evolution of position (left) and velocity (right) accuracy (truth − estimate) plotted with 3-σ covariance envelopes (dotted lines). Top plot is for the L_1 halo orbiter and the bottom is for the GEO satellite. The coordinates are given in the Earth-Moon synodic reference frame in the CRTBP [4].

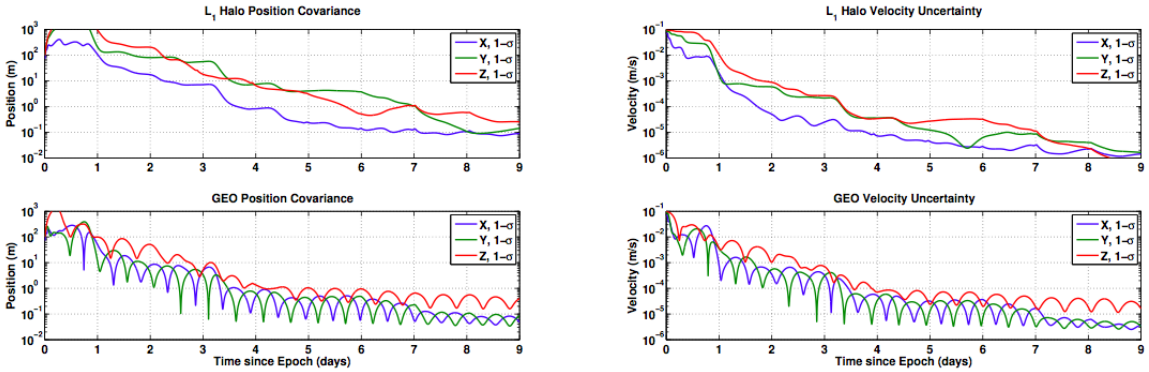

Figure 3. Time evolution of the position and velocity variance for the two satellites in the CRTBP [4].

2.2. Doppler Modeling

In this paper, we consider processing two-way Doppler measurements between the two constellation satellites. We model Doppler as a discrete range-rate: at each observation epoch, the incremental change in the roundtrip light path length (RTLPL) over a specified count time is divided by the count time. We assume a Newtonian model of light propagation, and thus the RTLPL is directly proportional to the roundtrip light time (RTLT) through the speed of light constant c. Given the position of the two spacecraft $\mathbf{r}_1(t)$, $\mathbf{r}_2(t)$ at time t, the one-way light time LT_{12} for a signal transmitted from spacecraft 1 to 2 at time t is found by solving the following equation

$$\mathrm{LT}_{12}(t) = \frac{\|\mathbf{r}_1(t) - \mathbf{r}_2[t + \mathrm{LT}_{12}(t)]\|}{c}, \tag{1}$$

where $\|\cdot\|$ indicates the vector norm. In many scenarios, LT_{12} must be solved for recursively. The simplest approach is to guess a value for LT_{12}, substitute into (1), and use the resulting value as the new guess to be substituted. Convergence is very good, with the solution changing by less than the machine precision after ~ 5 iterations. Furthermore, especially within a filter, numerically integrating the dynamics to find $\mathbf{r}_2[t + \mathrm{LT}_{12}(t)]$ becomes a large computational burden. For our

problem, $\mathrm{LT}_{12} \approx 1$ second, so a linear extrapolation is sufficient

$$\mathbf{r}_2[t + \mathrm{LT}_{12}(t)] \approx \mathbf{r}_2(t) + \mathbf{v}_2(t)\mathrm{LT}_{12}, \tag{2}$$

where $\mathbf{v}_2$ is the velocity of spacecraft 2. The RTLPL at observation epoch t is expressed as

$$\mathrm{RTLPL}(t) = c\left\{\mathrm{LT}_{12}(t) + \mathrm{LT}_{21}[t + \mathrm{LT}_{12}(\mathrm{t})]\right\}. \tag{3}$$

Finally, the discrete range-rate observation $g(t)$ at time t integrated over $[t - T_c, t]$ plus observational error $\epsilon(t)$ and bias $\bar{\epsilon}(t)$ is

$$g(t) = \frac{\mathrm{RTLPL}(t) - \mathrm{RTLPL}(t - T_c)}{T_c} + \epsilon(t) + \bar{\epsilon}(t). \tag{4}$$

The partial derivative $\tilde{H}$ of the observations with respect to the states $\mathbf{X}$ is obtained numerically via a central difference approximation. That is, for some small h,

$$\tilde{H} = \frac{\partial g}{\partial \mathbf{X}} \approx \frac{g(\mathbf{X} + h) - g(\mathbf{X} - h)}{2h}. \tag{5}$$

Choosing h too small can introduce major numerical errors, whereas choosing h too large makes this linear approximation of the derivative inaccurate. The approximate derivative should first be solved for over a range of h and a h value chosen in the subset where the approximation is the most stable.

2.3. Gravitational Perturbations in the Earth-Moon System

In the real solar system, the Lagrange points shift in position relative to the Earth and Moon on account of the Moon's non-circular orbit about the Earth and other perturbations in the solar system. Given that the Earth-Moon three body system is chaotic, dynamical errors may cause the truth trajectory to rapidly drift away from the filter reference orbit and degrade the estimate. In this section, we discuss gravitational deviations of the Earth-Moon system from the CRTBP as well as the mathematical models implemented in our simulation.

- *n*-body forces
  n-body forces are caused by celestial bodies not included in the Earth-Moon three body problem, such as the sun and other planets in the solar system. The acceleration $\ddot{\mathbf{r}}_i$ of the spacecraft due to the point-mass gravitation of body i is given as

$$\ddot{\mathbf{r}}_i = -\mu_i \left[\frac{\mathfrak{r}_i}{\mathfrak{r}_i^3} + \frac{\mathbf{R}_i}{R_i^3}\right], \tag{6}$$

  where $\mathfrak{r}_i$ is a vector pointing from body i to the spacecraft and $\mathbf{R}_i$ is a vector pointing from the Earth to body i [8]. The positions of celestial bodies are computed based on JPL's DE 405 ephemerides and thus are no longer constrained to be in a circular orbit [9, 10].

- Non-spherical Earth gravity field
  The Earth's gravitational potential is given in terms of spherical harmonics as

$$U = \frac{\mu}{r}\left[1 - \sum_{l=2}^{\infty} J_l \left(\frac{\mathscr{R}}{r}\right)^l P_l(\sin\varphi_{\rm gc}) + \sum_{l=2}^{\infty}\sum_{m=1}^{l}\left(\frac{\mathscr{R}}{r}\right)^l P_{l,m}(\sin\phi_{\rm gc})\left\{C_{l,m}\cos(m\lambda) + S_{l,m}\sin(m\lambda)\right\}\right], \quad (7)$$

  where $\mathscr{R}$ is the radius of the Earth, r is the distance between the spacecraft and the center of the Earth, λ is the longitude of the satellite, $\phi_{\rm gc}$ is the geocentric latitude of the satellite, P_l are the Legendre polynomials, $P_{l,m}$ are the associated Legendre polynomials of degree l and order m, and J_l, $C_{l,m}$ and $S_{l,m}$ are harmonic coefficients. In this paper, we use the GRACE Gravity Model 02 constrained with terrestrial gravity information (GGM02C) for these coefficients [11]. The acceleration $\ddot{\mathbf{r}}$ due to the non-spherical central body is given simply as $\ddot{\mathbf{r}} = -\nabla U$ and is applied to the GEO satellite in place of the point-mass model discussed above. The most notable effect of a non-spherical gravity model is the secular precession of the orbital plane, but all orbital elements are also nominally affected in a periodic fashion [12].

3. Method

In this section, we explain the details of our simulation setup, such as initial states, the a priori state uncertainty, measurement errors, and filter parameters. We simulate a two satellite LiAISON configuration with one satellite in an Earth-Moon L_1 halo orbit and the other in a GEO orbit. For all cases, a truth trajectory (without errors) is first generated using JPL's MONTE software: initial states and their associated a priori covariances for all cases are listed in Table 1. Based on this truth trajectory, the Doppler data (simulated as discrete range-rate measurements) is generated according to the model described in Section 2.2.. Additional observation parameters are listed in Table 2. Note that decreasing the observation interval to 100 s as in the example in Section 2.1. does not improve filter convergence or accuracy but increases computational burden significantly. The reference orbit will include deviations in the initial conditions as listed in Table 3.

Table 1. Initial truth states for the two satellites and their associated a priori variance values ("1-σ"). All a priori state correlations are assumed to be 0.

	X_0 [m]	Y_0 [m]	Z_0 [m]	$\dot{X}_0$ [m/s]	$\dot{Y}_0$ [m/s]	$\dot{Z}_0$ [m/s]
L_1	3.33321×10^8	-7.61342×10^7	-2.08739×10^7	2.57178×10^2	9.30274×10^2	3.46177×10^2
GEO	4.21600×10^7	0	0	0	3.07497×10^3	5.36683×10^{-1}
1-σ	1.00000×10^4	1.00000×10^4	1.00000×10^4	1.00000×10^1	1.00000×10^1	1.00000×10^1

Table 2. Observation parameters for all simulations cases.

Epoch	Interval [s]	Arc length [days]
2020/01/01	1.00000×10^3	1.99957×10^1

Table 3. Initial state deviation values common to all simulation cases.

	x_0 [m]	y_0 [m]	z_0 [m]	Norm [m]
Halo	8.19032×10^1	5.67041×10^1	8.74653×10^0	1.00000×10^2
GEO	1.14857×10^1	7.07301×10^1	6.97518×10^1	1.00000×10^2

	$\dot{x}_0$ [m/s]	$\dot{y}_0$ [m/s]	$\dot{z}_0$ [m/s]	Norm [km/s]
Halo	2.44876×10^{-3}	4.80858×10^{-3}	8.41909×10^{-3}	1.00000×10^{-2}
GEO	5.12723×10^{-3}	8.45370×10^{-3}	1.49881×10^{-3}	1.00000×10^{-2}

The observations were processed using an extended Kalman filter (EKF). The state vector $\mathbf{X}(t)$ at time t is defined as

$$\mathbf{X}(t) = [\mathbf{r}_1(t) \quad \mathbf{v}_1(t) \quad \mathbf{r}_2(t) \quad \mathbf{v}_2(t) \quad \bar{\epsilon}], \tag{8}$$

where all variables are defined in Section 2.2.. Again, the bias is assumed to be constant in both the filter model and the truth trajectory. To improve numerical stability, the Joseph covariance update is implemented

$$P = (\mathrm{I} - K_k \tilde{H}_k)\bar{P}_k(\mathrm{I} - K_k \tilde{H}_k)^{\mathrm{T}} + K_k R_k K_k^{\mathrm{T}}, \tag{9}$$

where the subscript indicates the observation number, P is the measurement updated covariance, K is the Kalman gain, $\tilde{H}$ is the linear relationship between the state and the observations, and $\bar{P}$ is the time updated covariance. Furthermore, state noise compensation (SNC) is implemented for white Gaussian process noise on the accelerations with constant diffusion. If we assume that the observations are dense enough such that the velocity is constant over an observation interval, the covariance time update per spacecraft is modified as

$$\bar{P}_{k+1} = \Phi(t_{k+1}, t_k) P_k \Phi^{\mathrm{T}}(t_{k+1}, t_k) + \Gamma(t_{k+1}, t_k) Q \Gamma^{\mathrm{T}}(t_{k+1}, t_k) \tag{10}$$

$$\Gamma(t_{k+1}, t_k) = \Delta t \begin{bmatrix} \Delta t/2 \cdot \mathrm{I}_{3\times3} \\ \mathrm{I}_{3\times3} \end{bmatrix}. \tag{11}$$

SNC acts to inflate the covariance matrix so that, especially in the presence of unmodeled accelerations, the filter does not saturate before a good state estimate is achieved [13]. We set $Q = 4 \times 10^{-14} \cdot \mathrm{I}_{3\times3}$ $(\mathrm{m/s^2})^2$ for this paper. A more thorough discussion on the filtering techniques used can be found in Parker, et al. and Leonard, et al [4, 5].

The numerical integrator used is a variable step Runge-Kutta integrator that compares the results of 7th and 8th order integrations to adjust the step size. The initial guess for the time step is 10^{-7} and the tolerance used to compare the 7th and 8th order results is 10^{-14}. State transition matrices are computed numerically along with the state parameters. All integrators, derivative functions for the integrators, and implementation of the DE 405 ephemerides were provided by the TurboProp software suite [14].

Based on Thornton and Border, we set the nominal Doppler error to 1 mm/s 1-σ and the bias to a constant 0.2 mm/s to account for solar plasma fluctuations, solar plasma drift, and instrument instabilities for an S-band signal. For X-band, the error is reduced to 0.1 mm/s 1-σ and the bias to a constant 0.02 mm/s as the plasma effects are about an order of magnitude smaller [15]. In both

cases, the error is modeled as white Gaussian noise and the filter variance input for the observation noise was set at the 1-σ noise level for each transmission frequency. Occultation of the tracking signal due to the Earth is considered. In addition, in order to improve filter stability, tracking is deliberately turned off when the estimated absolute velocity in the x-direction of the GEO satellite is less than 1.50000×10^3 m/s. Future work is to determine theoretically why such a singularity exists when processing Doppler measurements but not instantaneous range and range-rate measurements.

To introduce dynamical modeling errors, in addition to the initial state errors, we consider the following.

- The gravitational acceleration due to all planets in the solar system plus the sun is included in the truth trajectory, whereas only the gravity due to the sun, the moon, and the Earth are modeled in the filter
- A 20×20 gravity field is assumed for the truth trajectory, whereas the filter only implements a 5×5 model

We expect these accelerations to be accounted for in the filter by the SNC algorithm described previously. Although solar radiation pressure was not included in the current analysis, previous work suggests that its effect on the state estimate accuracy is small; i.e. on the order of $10^1 \sim 10^2$ meters for an coefficient of reflectivity error of 20% [5].

4. Results

In this section, we discuss the navigation simulation results. In addition to the two transmission frequencies, we test a case where we assume the L_1 satellite's state is well determined, for instance through groundtracking, and thus is not estimated.

4.1. Two-Way S-Band Doppler Tracking

Figures 4–7 and Table 4 summarize the filtering result for the complete state estimation using S-band Doppler tracking. Note that accuracy is defined as (truth) − (filtered). We find that the variance of the states stabilize after approximately a week of tracking, which is comparable to the results obtained in the CRTBP. Both the variance values after convergence and the state estimate accuracy, however, are about 2 orders of magnitude worse than in the baseline CRTBP simulation. This result is expected as range-rate is a weaker observation type than range [13]. In addition, the accuracy after 20 days of measurement processing is better than the initial state deviation introduced. Unlike the states, the estimate of the observation bias does not converge in a week. The closing of the covariance bounds, however, suggests that information does exist in the observations and that a longer data arc should result in a better estimate. We conclude that LiAISON is indeed effective in processing the discrete change in relative RTLPL to improve the absolute state knowledge of both satellites in the constellation.

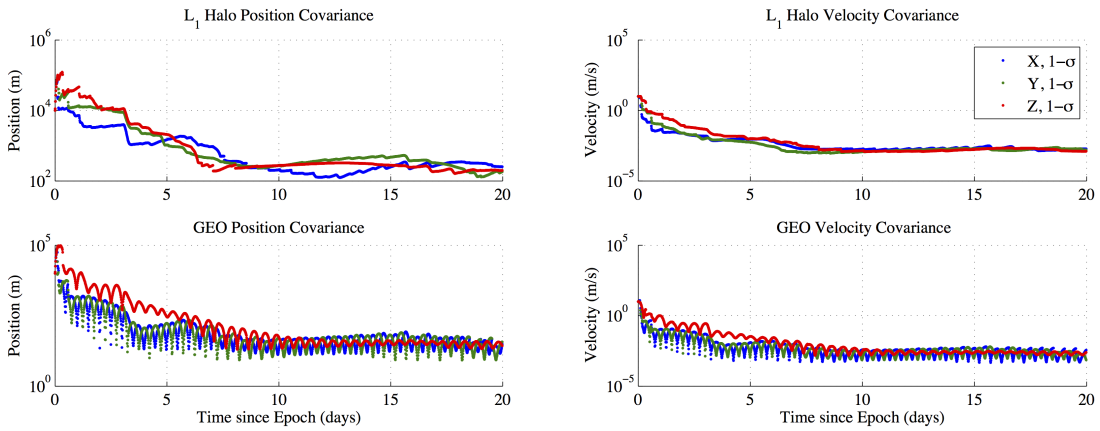

Figure 4. Position (left) and velocity (right) standard deviation history of both the L_1 (top) and GEO (bottom) satellites for S-band Doppler tracking. 1-σ values are shown for each cartesian direction.

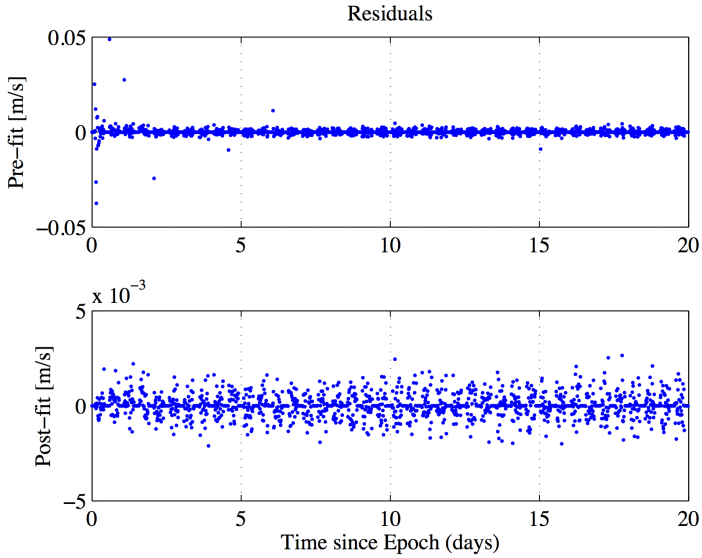

Figure 5. Pre-fit (top) and post-fit (bottom) residual history for S-band Doppler tracking. RMS of the post-fit residuals is 7.02350×10^{-4} m/s.

Table 4. Accuracy RMS values for the L_1 (top) and GEO (bottom) satellites in each cartesian direction of the last half of the filter run for S-band Doppler tracking. The "3D" value is the RMS of the RMSs in the individual coordinates.

	X	**Y**	**Z**	**3D**
L_1 Pos [m]	1.18084×10^{2}	1.69900×10^{2}	2.07601×10^{2}	2.93100×10^{2}
L_1 Vel [m/s]	8.70607×10^{-4}	1.28107×10^{-3}	1.39422×10^{-3}	2.08398×10^{-3}

	X	**Y**	**Z**	**3D**
GEO Pos [m]	5.10852×10^{1}	5.21260×10^{1}	1.74052×10^{1}	7.50317×10^{1}
GEO Vel [m/s]	3.77122×10^{-3}	3.72236×10^{-3}	1.27867×10^{-3}	5.45097×10^{-3}

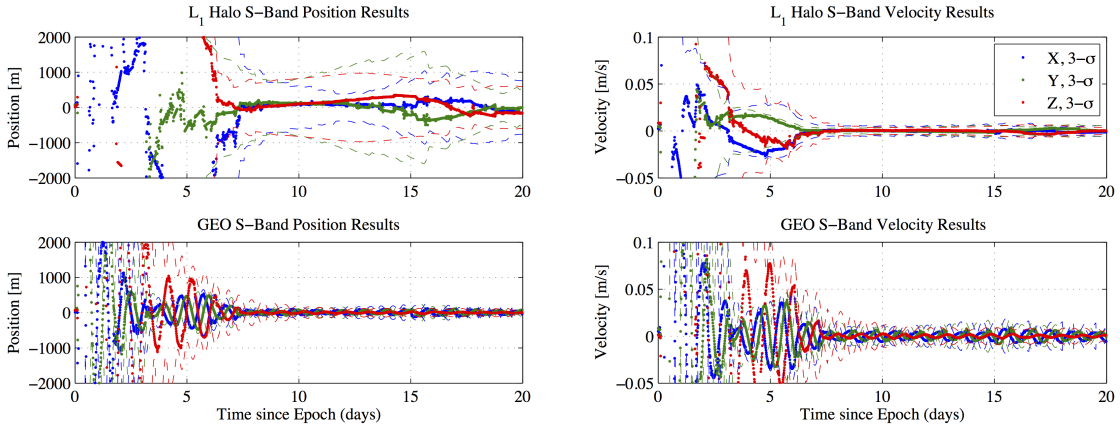

Figure 6. Position (left) and velocity (right) estimation accuracy of both the L_1 (top) and GEO (bottom) satellites for S-band Doppler tracking. The 3-σ covariance bounds are plotted as dashed lines.

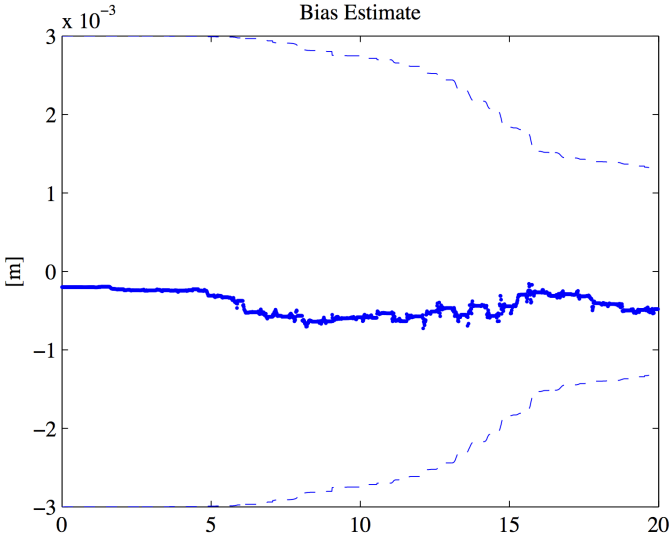

Figure 7. Observation bias estimation accuracy for S-band Doppler tracking. The 3-σ covariance bounds are plotted as dashed lines.

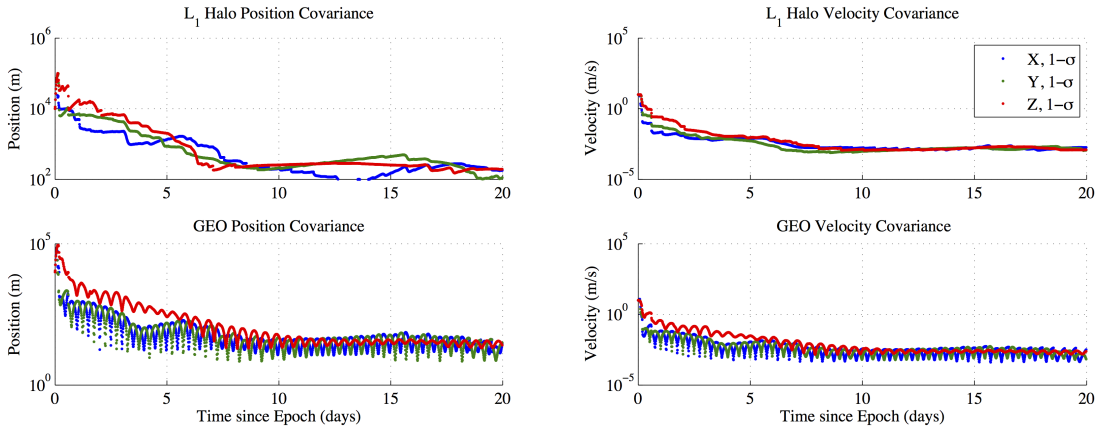

Figure 8. Position (left) and velocity (right) standard deviation history of both the L_1 (top) and GEO (bottom) satellites for X-band Doppler tracking. 1-σ values are shown for each cartesian direction.

4.2. Two-Way X-Band Doppler Tracking

Figures 8–9 and Table 4 summarize the filtering result for the complete state estimation using X-band Doppler tracking. The RMS of the post-fit residuals is 2.03368×10^{-5} m/s. Compared to the S-band results, the covariance convergence is slightly better due to the tighter observation variance bound R. The state estimate accuracy, however, is almost identical. Furthermore, since the observation bias is so small, the effects of bias are comparable to the unmodeled accelerations considered via SNC, and thus its observability is very limited. Regarding the simulation results presented here, there is no distinct advantage in choosing X-band tracking over S-band.

Table 5. Accuracy RMS values for the L_1 (top) and GEO (bottom) satellites in each cartesian direction of the last half of the filter run for X-band Doppler tracking. The "3D" value is the RMS of the RMSs in the individual coordinates.

	X	**Y**	**Z**	**3D**
L_1 Pos [m]	1.32688×10^{2}	1.78178×10^{2}	1.95075×10^{2}	2.95648×10^{2}
L_1 Vel [m/s]	8.16778×10^{-4}	1.34813×10^{-3}	1.52667×10^{-3}	2.19439×10^{-3}
	X	**Y**	**Z**	**3D**
GEO Pos [m]	5.35849×10^{1}	5.35001×10^{1}	2.31763×10^{1}	7.91881×10^{1}
GEO Vel [m/s]	3.88276×10^{-3}	3.89408×10^{-3}	1.69971×10^{-3}	5.75576×10^{-3}

4.3. Two-Way S-Band Doppler Tracking With Perfect L_1 State Knowledge

By assuming perfect state knowledge of the L_1 satellite, which can be achieved by simply reducing the a priori covariance of these states to 0, we may use all of the information in the observations to estimate the state of the GEO satellite. As such, we expect improved navigation performance. Figures 10–11 and Table 6 summarize the filtering result. The state variances indeed collapse much faster than the previous cases, stabilizing after only a couple of days of tracking. The covariance bounds, however, are not any smaller, and neither is the state estimate accuracy any better. This

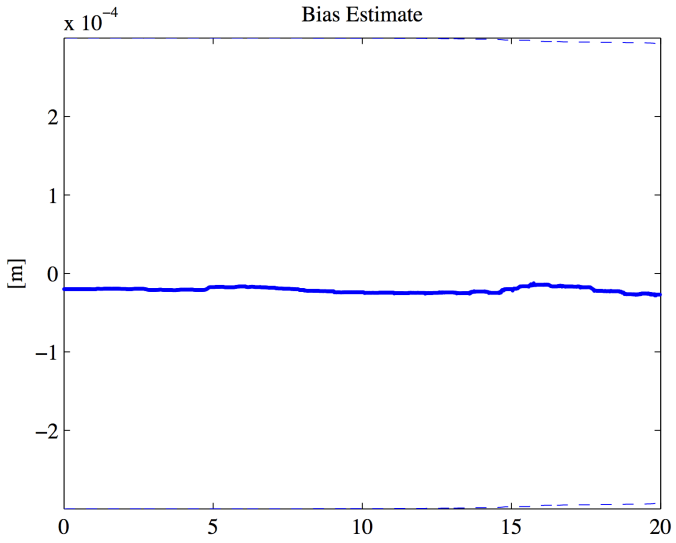

Figure 9. Observation bias estimation accuracy for X-band Doppler tracking. The 3-σ covariance bounds are plotted as dashed lines.

Table 6. Accuracy RMS values for the GEO satellite in each cartesian direction of the last half of the filter run for S-band Doppler tracking with perfect state knowledge of the L_1 satellite. The "3D" value is the RMS of the RMSs in the individual coordinates.

	X	**Y**	**Z**	**3D**
GEO Pos [m]	4.92068×10^{1}	5.16604×10^{1}	3.45135×10^{1}	7.92546×10^{1}
GEO Vel [m/s]	3.76825×10^{-3}	3.54303×10^{-3}	2.45439×10^{-3}	5.72511×10^{-3}

results suggests a fundamental limit to the amount of state information that can be extracted with the current filter setup. Future work is to corroborate this finding via a Cramer-Rao analysis and to consider other methods of processing Doppler observations such as treating it as an accumulated range measurement [4]. Information regarding the observation bias, on the other hand, does increase significantly with the perfect knowledge assumption. The estimate accuracy is poor only because growing errors in the numerical integration are being imposed upon the bias in order to reduce residuals. Therefore, observability of the bias may be improved by reducing the state uncertainty of one of the satellites; e.g. combining groundtracks to this LiAISON configuration.

5. Conclusions

In this paper, simulation results of an autonomous navigation concept were presented, where the absolute state of satellites are estimated via relative measurements only. The method leverages asymmetry in the force model and thus is apt for applications that include libration point orbits. Relative two-way Doppler measurements with errors corresponding to S- and X-band were simulated as discrete range-rates over a specified count time. Although filter accuracy is worse than when processing range data due to the inherent weakness of range-rate type observations, all filters converge and provide state estimates with $\sim 10^{2}$ meter level accuracy in position and $\sim 10^{-3}$

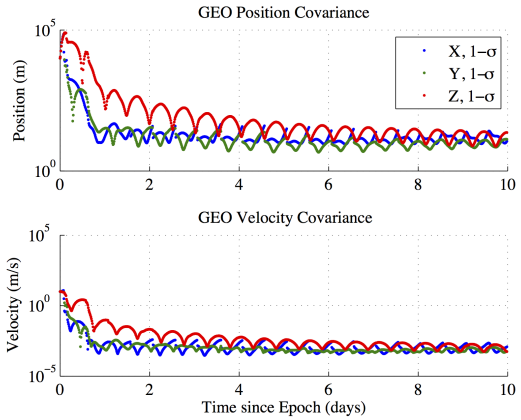

Figure 10. Position (top) and velocity (bottom) standard deviation history of the GEO satellite for S-band Doppler tracking with perfect state knowledge of the L_1 satellite. 1-σ values are shown for each cartesian direction.

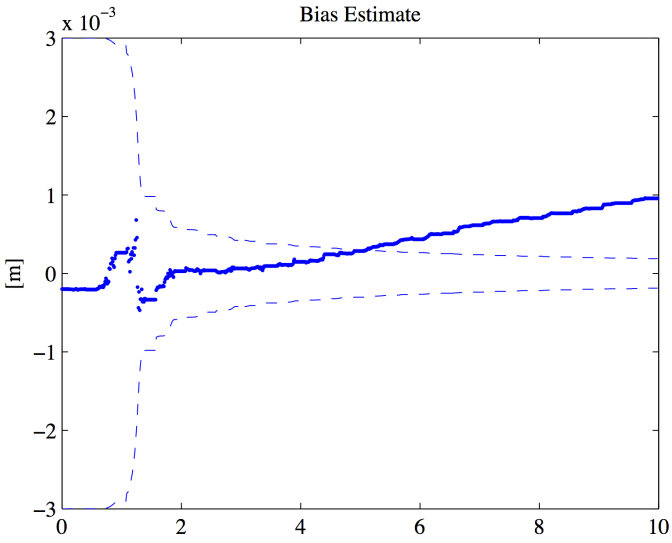

Figure 11. Observation bias estimation accuracy for S-band Doppler tracking with perfect state knowledge of the L_1 satellite. The 3-σ covariance bounds are plotted as dashed lines.

m/s accuracy in velocity. Future work is to determine theoretically the singularities unique to processing range-rate-type measurements as well as investigating better ways of filtering the Doppler information.

6. Acknowledgements

The research presented in this paper has been carried out at the Jet Propulsion Laboratory, California Institute of Technology, under a contract with the National Aeronautics and Space Administration.

7. References

[1] Hill, K. Autonomous Navigation in Libration Point Orbits. Ph.D. thesis, Graduate School of the University of Colorado, 2007.

[2] Hill, K. and Born, G. H. "Autonomous Interplanetary Orbit Determination Using Satellite-to-Satellite Tracking." Journal of Guidance, Control, and Dynamics, Vol. 30, No. 3, pp. 679–686, 2007.

[3] Villac, B., Chow, C., Lo, M., Hintz, G., and Nazari, Z. "Dynamic Optimization of Multi-Spacecraft Relative Navigation Configurations in the Earth-Moon System." 2010. Presented at the *George H. Born Symposium*, Boulder, CO.

[4] Parker, J. S., Anderson, R. L., Born, G. H., and Fujimoto, K. "Navigation Between Geosynchronous And Lunar L1 Orbiters." 2012. Presented at the *2012 AIAA/AAS Astrodynamics Specialist Conference*, Minneapolis, MN.

[5] Leonard, J. M., McGranaghan, R. M., Fujimoto, K., Born, G. H., Parker, J. S., and Anderson, R. L. "LiAISON-Supplemented Navigation For Geosynchronous and Lunar L1 Orbiters." 2012. Presented at the *2012 AIAA/AAS Astrodynamics Specialist Conference*, Minneapolis, MN.

[6] Hill, K., Lo, M. W., and Born, G. H. "Linked, Autonomous, Interplanetary Satellite Orbit Navigation (LiAISON)." 2005. Presented at the *AAS/AIAA Astrodynamics Specialist Conference*, Lake Tahoe, CA. AAS 05-399.

[7] Hill, K., Parker, J. S., Born, G. H., and Demandante, N. "A Lunar L2 Navigation, Communication, and Gravity Mission." 2006. Presented at the *2006 AIAA/AAS Astrodynamics Specialist Conference*, Keystone, Colorado, AIAA 2006-6662.

[8] Roy, A. E. Orbital Motion. Taylor & Francis Group, New York, NY, 2005.

[9] Standish, E. M. "JPL Planetary and Lunar Ephemerides, DE405/LE405." Interoffice memorandum, Jet Propulsion Laboratory, 1998. IOM 312F-98-048.

[10] Hoffman, D. A. "A Set of C Utility Programs for Processing JPL Ephemeris Data." Tech. rep., NASA Johnson Space Center, 1998.

[11] Tapley, B., Ries, J., Bettadpur, S., Chambers, D., Cheng, M., Condi, F., Gunter, B., Kang, Z., Nagel, P., Pastor, R., Pekker, T., Poole, S., and Wang, F. "GGM02 - An improved Earth gravity field model from GRACE." Journal of Geodesy, 2005.

[12] Vallado, D. Fundamentals of Astrodyamics and Applications. Microcosm Press, Hawthorne, CA, third edn., 2007.

[13] Tapley, B. D., Schutz, B. E., and Born, G. H. Statistical Orbit Determination. Elsevier Academic Press, Burlington, MA, 2004. Pp. 159-284.

[14] Hill, K. and Jones, B. A. "TurboProp Version 4.0." Tech. rep., Colorado Center for Astrodynamics Research, 2009.

[15] Thornton, C. L. and Border, J. S. "Radiometric Tracking Techniques for Deep-Space Navigation." Tech. rep., Jet Propulsion Laboratory, 2000. Monograph 1, Deep-Space Communications And Navigation Series. JPL Publication 00-11.